JOURNAL OF APPLIED PHYSICS **123**, 174903 (2018)

Seismic isolation of buildings using composite foundations based on metamaterials

O. Casablanca,[1] G. Ventura,[2] F. Garescì,[1] B. Azzerboni,[1] B. Chiaia,[2] M. Chiappini,[3] and G. Finocchio[4,a)]
[1]*Department of Engineering, University of Messina, I-98166 Messina, Italy*
[2]*Politecnino di Torino, Torino, Italy*
[3]*Istituto Nazionale di Geofisica e Vulcanologia (INGV), Via Vigna Murata 605, 00143 Roma, Italy*
[4]*Department of Mathematical and Computer Sciences, Physical Sciences and Earth Sciences, University of Messina, I-98166 Messina, Italy*

(Received 2 December 2017; accepted 7 April 2018; published online 3 May 2018)

Metamaterials can be engineered to interact with waves in entirely new ways, finding application on the nanoscale in various fields such as optics and acoustics. In addition, acoustic metamaterials can be used in large-scale experiments for filtering and manipulating seismic waves (seismic metamaterials). Here, we propose seismic isolation based on a device that combines some properties of seismic metamaterials (e.g., periodic mass-in-mass systems) with that of a standard foundation positioned right below the building for isolation purposes. The concepts on which this solution is based are the local resonance and a dual-stiffness structure that preserves large (small) rigidity for compression (shear) effects. In other words, this paper introduces a different approach to seismic isolation by using certain principles of seismic metamaterials. The experimental demonstrator tested on the laboratory scale exhibits a spectral bandgap that begins at 4.5 Hz. Within the bandgap, it filters more than 50% of the seismic energy via an internal dissipation process. Our results open a path toward the seismic resilience of buildings and a critical infrastructure to shear seismic waves, achieving higher efficiency compared to traditional seismic insulators and passive energy-dissipation systems. https://doi.org/10.1063/1.5018005

I. INTRODUCTION

The concept of metamaterials has emerged in recent years for developing materials with unique properties not generally found in nature. Although the idea was developed originally in the context of electromagnetic field theory,[1,2] a subfield focusing on elastic metamaterials seems to be promising for medical applications, seismology, superlenses, imaging, etc.[3] Elastic metamaterials with appropriate locally resonant structures can filter the energy of propagating waves with frequencies in a stopband region. The first experimental evidence of this property is found in Liu *et al.*,[4] who fabricated sonic crystals with a simple microstructure unit consisting of a lead sphere with the coating of an elastically soft material (i.e., silicon rubber) that exhibited a main stopband frequency region tuned near the resonant frequency of 400 Hz. Acting as internal resonators, the lead spheres had a constant spatial lattice that was two orders of magnitude smaller than the relevant wavelength at the resonant frequency. The use of metamaterials to manipulate seismic waves, which are characterized by volume [primary (P) and secondary (S)] and surface (Rayleigh and Love) waves, has been demonstrated for Rayleigh-type waves through a series of full-scale experiments.[5–7] Basically, it has been shown that seismic metamaterials with sub-wavelength local resonators can be designed to have a negative mass density and/or a negative Young's modulus as a way to control elastic wave propagation within the frequency range of seismic waves (<50 Hz). In particular, Brûlé *et al.*[5] reported modifying the seismic energy distribution in the presence of a regular mesh of vertical cylindrical voids. Colombi *et al.*[6] pointed out that trees in a forest can be used as natural metamaterials, and other proposed approaches involve developing large-scale phononic metamaterials.[8,9]

The aforementioned research focused on controlling the propagation of seismic waves to protect the critical infrastructure via a seismic invisibility cloak. However, such solutions require an amount of space that is comparable to the region being cloaked, and they were developed mainly for surface seismic waves. A different approach has been proposed,[10] in which a vibrating barrier in the form of a dummy building absorbs a significant portion of the dynamic energy of a seismic wave. Meanwhile, other strategies for vibration control based on seismic isolation (SI) devices lead to significant advantages from a strong reduction in seismic vulnerability due to modifying the dynamic structural characteristics by (i) increasing the dissipative properties of the structure and/or (ii) altering its rigidity and thereby shifting the structural frequencies. However, standard isolation strategies perform less well in protecting tall buildings or if the soil below the building is soft.[11] In addition, for civil engineering applications, seismic isolation should work for frequencies below 10 Hz.[12]

Here, we introduce the concept of a "composite foundation" (CF) that integrates the physics of seismic

a)Email: gfinocchio@unime.it

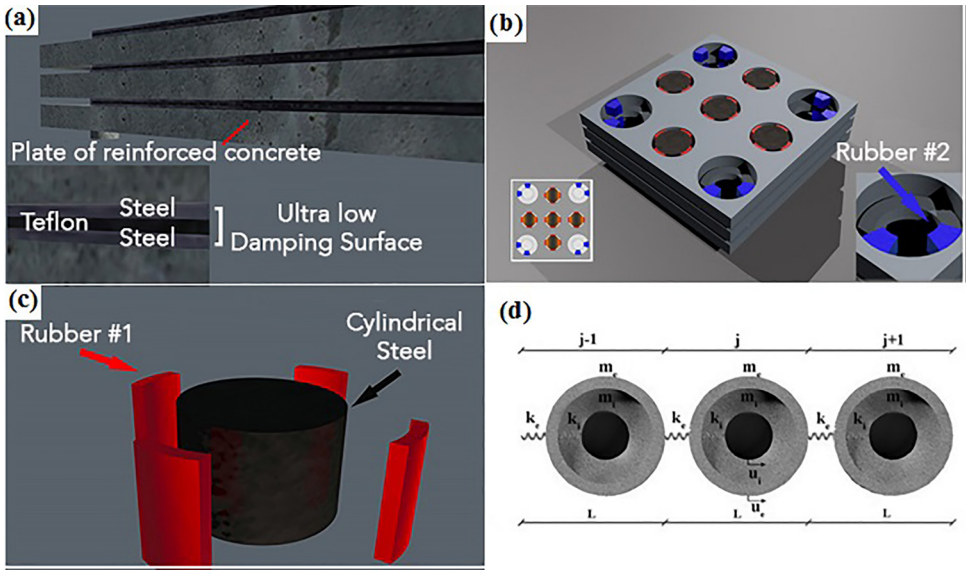

FIG. 1. Schematics of composite foundation (CF) studied herein. (a) Plates and a magnified view of their disconnection element. (b) Spatial distribution of resonators and the detail of the elastomeric element used to connect different plates. (c) Example of a resonator and an elastomeric element separating the steel resonator mass from the concrete plate. (d) A schematic of a periodic mass-in-mass system with the indication of m_i, m_e, k_i, and k_e; u_e and u_i are the displacements of the external and internal masses, respectively, while L is the spatial period of the CF in the vertical direction (see also Table I).

metamaterials based on the concept of periodic mass-in-mass systems directly with the foundation of a building, creating on-site filters that reduce the energy transferred from a seismic wave to the building at frequencies in the range of the first vibration mode of the building itself. The use of CFs represents a new paradigm for designing seismic protection.[13] We focus on S-waves because of the fact that their relatively high amplitudes are often associated with basin resonances and other ground-filtering mechanisms (e.g., Love waves). Our results introduce a new way to design seismic insulation by using the fundamental properties of seismic metamaterials.

II. MATERIALS AND METHODS

A. Composite foundation

A sketch of the device under investigation is shown in Fig. 1. It comprises four reinforced concrete plates with a square cross-section of side 1 m and a thickness of 20 cm [Fig. 1(a)]. Each plate is disconnected from the others by means of an ultralow damping surface realized by a suitable combination of layers of steel and Teflon [Fig. 1(a)]. Each plate has a matrix of nine cylindrical inclusions with a regular spatial distribution and a center-to-center distance $d_C = 30$ cm between adjacent inclusions. Mechanical connections comprising rubber with low Young's modulus and a steel tube are fixed at the four corner inclusions (diameter of 15 cm) to connect neighboring plates [Fig. 1(b)]. The other inclusions are used to host steel cylinders and rubbers (rubber #1) as shown in Fig. 1(c) to allow them to act as internal resonators. Along with the damping due to the rubber, the presence in the CF of spatially ordered local resonators with a dimension smaller than the wavelength of propagating waves allows sub-wavelength wave manipulation similar to that reported previously.[4] Figure 2 shows schematically an example of a CF below a building for the purpose of protection. The plates with internal resonators are sandwiched between a load-distribution plate and a foundation plate to give a more-uniform load distribution on the CF and hence improve its dynamic response.

B. Equivalence of composite foundations with periodic mass-in-mass systems

The working principle behind CFs is that of a periodic mass-in-mass system[14–18] without a damper, as discussed below in detail. Considering the dynamical system in Fig. 1(d), the total energy E^j of element j is given by the sum of kinetic (E_K^j) and potential (V_P^j) energies

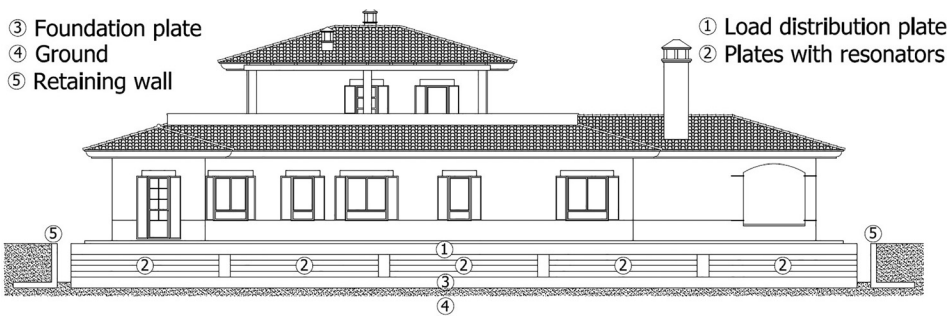

FIG. 2. Schematic of CF (plates with resonators) below a building that is being protected. This device is clearly a part of the foundation itself and is located between a load-distribution plate and a foundation plate.

$$E^j = E_K^j + V_P^j = \frac{1}{2}m_i\dot{u}_i^{j} + \frac{1}{2}m_e\dot{u}_e^{j} + \frac{1}{2}k_i(u_i^j - u_e^j)^2 + \frac{1}{2}k_e(u_e^j - u_e^{j-1})^2 + \frac{1}{2}k_e(u_e^{j+1} - u_e^j)^2, \quad (1)$$

where m and k are the mass and the spring constant, respectively, of the mass-in-mass system, the subscripts i and e relate to the internal mass and the external mass, respectively, and $\dot{u}$ and u are the velocity and the displacement of the mass, respectively. Given that the system is conservative, the dynamical equations computed as

$$\begin{cases} \dfrac{d}{dt}\left(\dfrac{\partial E_K}{\partial \dot{u}_i^j}\right) + \dfrac{\partial V_P}{\partial u_i^j} = 0, \\ \dfrac{d}{dt}\left(\dfrac{\partial E_K}{\partial \dot{u}_e^j}\right) + \dfrac{\partial V_P}{\partial u_e^j} = 0, \end{cases}$$

are

$$\begin{cases} m_e\ddot{u}_e^j + k_e(2u_e^j - u_e^{j-1} - u_e^{j+1}) + k_i(u_e^j - u_i^j) = 0, \\ m_i\ddot{u}_i^j + k_i(u_i^j - u_e^j) = 0. \end{cases} \quad (2)$$

By considering the harmonic wave solution (Bloch's theorem) for element j, the generic solution of Eq. (2) is

$$\begin{cases} u_i^{j+n} = B_i e^{i(qx+nqL-\omega t)}, \\ u_e^{j+n} = B_e e^{i(qx+nqL-\omega t)}, \end{cases} \quad (3)$$

where q is the wave number, ω is the angular frequency, L is the periodic spatial constant of the mass-in-mass system, and B_i and B_e are complex numbers that account for any offset phase between the two solutions. In Fourier space, the $j-1$ and $j+1$ generic solutions can be written in terms of the j generic solution

$$\begin{cases} u_1^{j-1} - - > U_1^j e^{i(-qL)}, \\ u_1^{j+1} - - > U_1^j e^{i(qL)}. \end{cases} \quad (4)$$

Combining Eqs. (2)–(5) with some trivial mathematical steps gives the dispersion relationship of a periodic mass-in-mass system[14,17]

$$m_e m_i\omega^4 - [k_i(m_e + m_i) + 2k_e m_i(1 - \cos qL)]\omega^2 + 2k_e k_i(1 - \cos qL) = 0. \quad (5)$$

The links between the discrete elements of the mass-in-mass system and the properties of the CF (periodicity along the vertical direction) are given in Table I. Considering the experimental parameters of the CF under test, the elements of the equivalent mass-in-mass system are $m_e = 317$ kg, $m_i = 245$ kg, $k_e = 155 \times 10^3$ N/m, $k_i = 1080 \times 10^3$ N/m (see Table I, right-hand column), and $L = 0.2$ m. The dispersion relationship computed as the roots of Eq. (1) shows a bandgap that begins at a frequency $f_{BG,i}$ near 5 Hz, where

$$f_{BG,i} = \frac{1}{2\pi}\sqrt{\frac{[k_i(m_e + m_i)]}{m_e m_i}} \quad (6)$$

and stops at a frequency $f_{BG,f}$ near 14 Hz, where

$$f_{BG,f} = \frac{1}{2\pi}\sqrt{\frac{[k_i(m_e + m_i) + 4k_e m_i] - \sqrt{[k_i(m_e + m_i) + 4k_e m_i]^2 - 16m_e m_i k_e k_i}}{2m_e m_i}}. \quad (7)$$

The results in Fig. 3 show that the analytical results [as computed with Eq. (1)] agree well with numerical computations of a full three-dimensional finite-element model of a CF comprising four plates that was discretized with tetrahedral finite elements (see the inset of Fig. 3 for the discretization used for the simulations). The device is considered to be a linear system[19–21] in which the plates are separated by an ideal disconnection element that simulates zero damping between the plates. This approximation is reasonable considering that the experimental data show a damping coefficient of around 3%. In addition, low damping does not modify the dispersion relationship.

C. Experimental system

A schematic of the measurement system and a photograph of the CF described above are shown in Figs. 4(a) and 4(b), respectively, with the key elements indicated; see also Figs. 1(a)–1(c). The input displacement is applied to the second plate (layer 2) by an MTS 204.71 actuator (Fig. 4). The bottom plate (fixed layer), which is disconnected via a low-damping multilayer from the second plate, is necessary for reducing the friction as much as possible. In a real building, it is necessary to use a load-distribution plate and a foundation plate to separate the active region of the CF (see Fig. 2). The measurement system is equipped with sensors to register (i) the displacement and the acceleration of each plate and (ii) the accelerations of the internal resonators. The data-acquisition system has 12 acceleration channels for layers 1–4, two voltage channels for the actuator, four channels for the slab displacements, 16 voltage channels for the resonator accelerometers (four plates, two resonators per plate, and two in-plane acceleration components), and eight voltage channels for the additional low-cost slab accelerometers, making a total of 42 channels with a sampling frequency of 100 Hz.

TABLE I. Conversion of parameters of the mass-in-mass system and the composite foundation (CF).

Mass-in-mass	Composite foundation	Conversion factors
m_e	Reinforced-concrete plate V_p (plate volume), ρ_c (concrete density)	$m_e = \rho_c \cdot V_p$ $\rho_c = 2400\,\mathrm{kg/m^3}$ $V_p = 13.21 \times 10^{-2}\,\mathrm{m^3}$
m_i	Steel cylinder n_c (number of cylinders), V_c (cylinder volume), ρ_s (concrete density)	$m_i = n_c \cdot \rho_s \cdot V_c$ $n_c = 5$ $\rho_s = 7800\,\mathrm{kg/m^3}$ $V_c = 6.28 \times 10^{-3}\mathrm{m^3}$
k_e	Rubber #1 (connection) E_{re} (Young's modulus of rubber), A_{re} (area of external element's rubber), L_{re} (length of external element's rubber)	$k_e = 2\frac{E_{re} \cdot A_{re}}{L_{re}}$ $E_{re} = 1.8 \times 10^6\mathrm{Pa}$ $A_{re} = 3.75 \times 10^{-3}\mathrm{m^2}$ $L_{re} = 8.75 \times 10^{-2}\mathrm{m}$
k_i	Rubber #2 (connection) E_{ri} (Young's modulus of rubber), A_{ri} (area of internal element's rubber), L_{ri} (length of internal element's rubber), n_c (number of cylinders)	$k_i = n_c\frac{E_{ri} \cdot A_{ri}}{L_{ri}}$ $n_c = 5$ $E_{ri} = 1.80 \times 10^6\mathrm{Pa}$ $A_{ri} = 3.00 \times 10^{-3}\mathrm{m^2}$ $L_{ri} = 2.50 \times 10^{-2}\mathrm{m}$

In detail, the plate displacements are acquired by four RDP LDC500A displacement transducers. These are inductive displacement sensors with integrated signal conditioning to output a voltage signal. These sensors were selected for their dynamic range when coupled with an electrodynamic actuator and a signal generator. This is a key aspect for correct measurements because the transducer is of the spring-return type, making it essential to verify that no detachment occurs between the sensor tip and the plate when the CF moves. The plate accelerations are measured by four PCB Piezotronics 356B18 triaxial accelerometers, exhibiting a sensitivity of 1000 mV/g and a frequency range of 0.5–3000 Hz. These accelerometers are based on a piezoelectric sensor element with built-in conditioning microelectronics and are characterized by high sensitivity and low spectral noise.[22] Because there is little space between the resonators and the concrete plate, the resonators are monitored during the test by using a special resin to glue the accelerometers to the upper surfaces of the resonators. For this application, the accelerometers "sacrificial," low-cost MEMS accelerometers are used. The selected accelerometers are Analog Devices model ADXL337, with a sensitivity of 300 mV/g and a voltage output. The printed circuit boards of these accelerometers are glued to the resonators with the interposition of insulation boards for short-circuit protection. We instrument two resonators per concrete plate and use four additional ADXL337 accelerometers to read the plate accelerations, in parallel to the four PCB Piezotronics triaxial accelerometers for redundancy and comparison purposes.

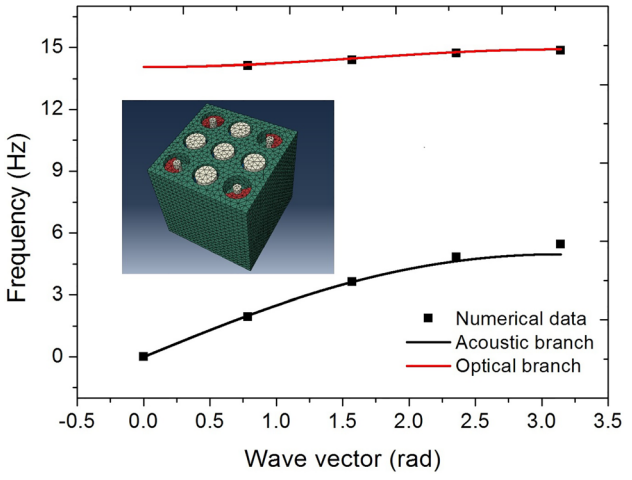

FIG. 3. Dispersion curve computed from the dispersion relationship [Eq. (1); solid lines] for periodic mass-in-mass systems ($L = 0.2$ m, $m_i = 317$ kg, $m_e = 245$ kg, $k_e = 155 \times 10^3$ N/m, and $k_i = 1080 \times 10^3$ N/m) and three-dimensional finite-element simulations (squares). The inset shows the three-dimensional finite-element discretization scheme used for the CF in which four plates are separated by an ideal disconnection plane.

III. RESULTS

Figure 5 summarizes the main results of the experimental measurements in response to a time-domain input displacement of the form $u_0 \sin(\omega t)$ with a nominal $u_0 = 3.5$ mm. This signal is applied to layer 1 at different frequencies ranging from 0.5 to 8 Hz. The sensors T1–T4, as indicated in the inset of Fig. 5(a), register a time-domain signal at the same frequency as that of the input signal, while the signal amplitude depends on the input frequency. Figure 5(a) shows the transfer function of the CF computed as the ratio of (i) the displacement amplitude measured by the sensor T4 to (ii) the input signal measured by T1. As the frequency approaches the beginning of the theoretical bandgap at 5 Hz (see Fig. 3), the signal propagating through the CF is attenuated. The attenuation coefficient as a function of frequency is shown in Fig. 5(b) (circles) as computed directly from the transfer function of Fig. 5(a) [see also Eq. (3)]. For completeness, Fig. 5(b) also shows the theoretical attenuation coefficient (solid line) displayed up to 8 Hz computed as the imaginary part of the wave vector qL given by

$$qL = a\cos\left(1 - \frac{m_e m_i \omega^4 - \omega^2 k_i (m_e + m_i)}{2\omega^2 k_e m_i - 2k_e k_i}\right). \quad (8)$$

Figures 5(c) and 5(d) show the time-domain traces as measured by sensors T1–T4 for input frequencies of 2 and 6 Hz, respectively. The data show clearly that inside the bandgap (6 Hz), the displacement is attenuated and the signal amplitude at T4 is reduced by more than 50% compared to the input signal at T1. Experiments performed with an additional weight of 1000 kg on top of the upper slab showed results that were quantitatively similar to those in Fig. 5. It should also be noted that any vibration of the building sitting on the CF will also be filtered at frequencies within its bandgap.

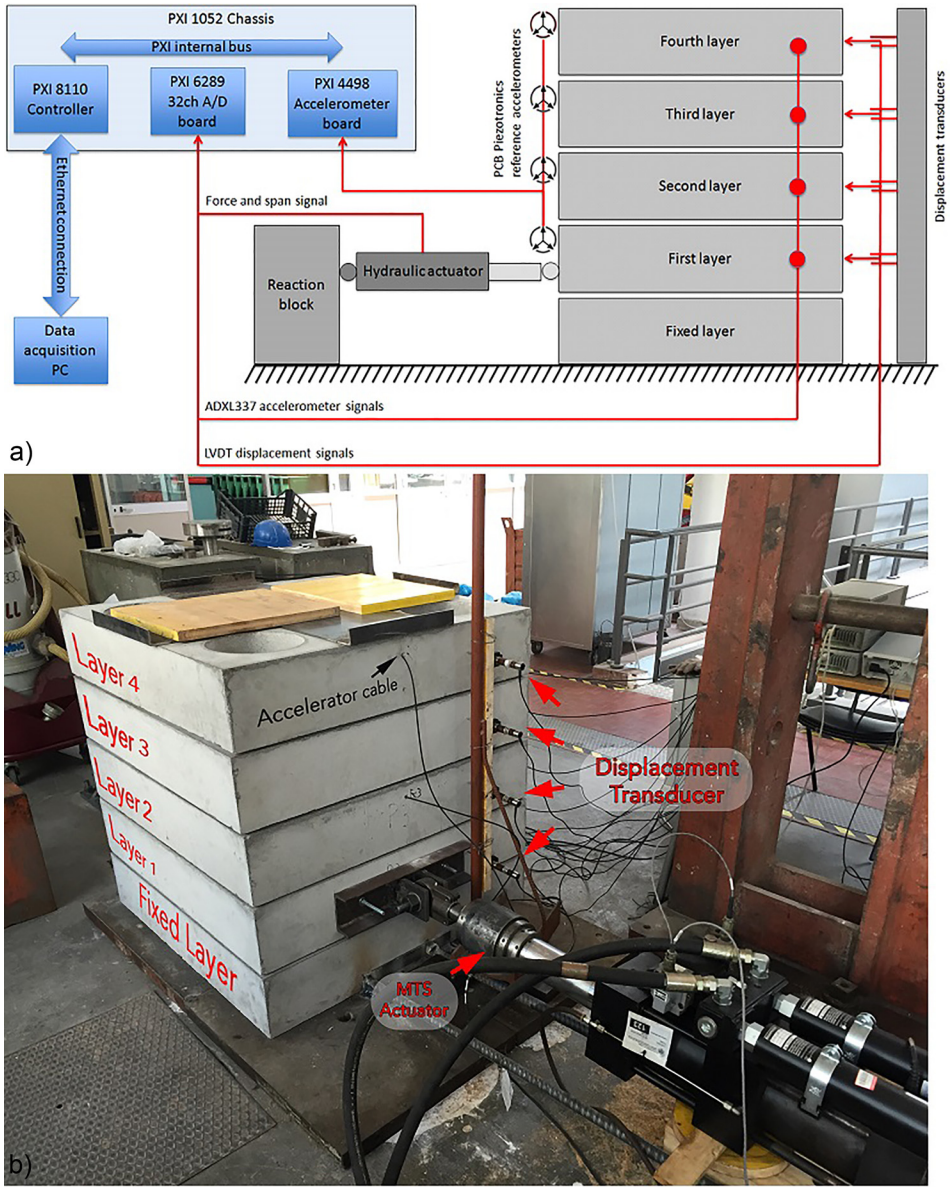

FIG. 4. (a) Schematic of the measurement system used for dynamic characterization of CF. (b) Photograph of CF under test, with main parts of the measurements system indicated. The device comprises four layers that are free to move over a fixed slab. Each layer is disconnected from others by an ultralow damping surface composed of steel (top surface) and steel/Teflon (bottom surface). All sensors used in the tests were sampled with a National Instruments system comprising a PXI-1052 chassis, a PXI-8110 embedded controller, a PXI-4498 board with 16 simultaneous sampling channels with 24-bit resolution to acquire the PCB Piezotronics accelerometer signals and a PXI-6289 board with 32 channels with 18-bit resolution for all voltage-output instruments, i.e., loads and spans at the MTS actuators, plate displacements for each layer, and resonator accelerations.

We consider the above results as proof of concept of the working principle of this CF (see the supplementary material for a video of the dynamic measurements). Even though the experimental study was performed by applying the displacement along one particular direction, we stress that because of the symmetry of the CF, its transfer function is independent of the S-wave polarization; in other words, it exhibits an isotropic response in the plane for its horizontal component.

To test the robustness of the CF, it was also subjected to an up-down chirp signal (for more than 10 min) characterized by a frequency that first increased from $f_0 = 1$ Hz to $f_M = 10$ Hz ($\Delta f = 9$ Hz) and then decreased to f_0 in $T = 10$ s

$$\begin{cases} s_{up}(t) = u_0(\omega)\sin\left(\omega_0 t + \dfrac{\Delta\omega}{T}t^2\right) & t \in \left[0, \dfrac{T}{2}\right], \\ s_{down}(t) = u_0(\omega)\sin\left(\omega_M t - \dfrac{\Delta\omega}{T}t^2\right) & t \in \left[\dfrac{T}{2}, T\right]. \end{cases} \tag{9}$$

Figure 6 shows the time-domain displacements of layers T1 and T4 for a complete cycle of the input signal. As the input frequency increases and approaches the bandgap, the displacement in layer T4 becomes less than that in layer T1. The frequency-dependent displacement in layer T4 (from a maximum of 6.6 mm at 1 Hz to a minimum of 3.8 mm at 10 Hz) is due to the limited dynamical response of the MTS actuator.

IV. DISCUSSION

In general, CFs differ markedly from ordinary seismic isolation devices. The seismic isolation property relates mainly to the ultralow-damping surface between different plates, whereas the additional key property coming from the metamaterial is the dissipation process due to the internal resonance (internal mass and spring), which is $f = \frac{1}{2\pi}\sqrt{\frac{k_i}{m_i}} = 9.2$ Hz in the present case [see Eq. (6)]. In particular, a CF acts as a filter with marked attenuation over a designed frequency range (bandgap), whereas a classical SI device introduces a shift in the natural oscillation periods of the building. This is a very important feature for buildings with long vibration periods: such buildings

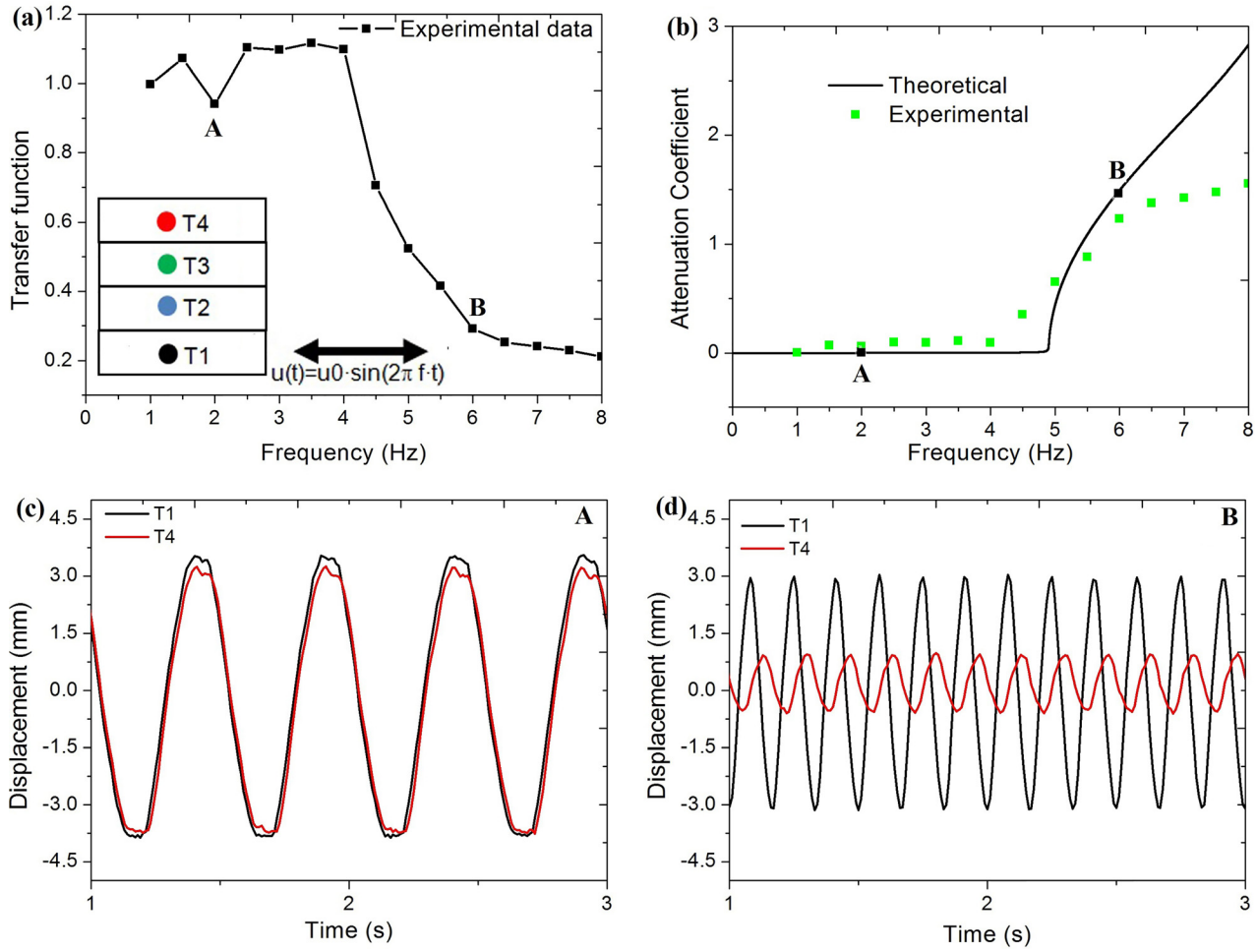

FIG. 5. (a) Transfer function of CF under test computed as the ratio of (i) the signal amplitude measured by T4 to (ii) that measured by T1 at different input frequencies. Inset: indication of the link between sensors T1–T4 and plates (T1 and T4 correspond to the input and output displacements, respectively). (b) Comparison between the theoretical attenuation coefficient (solid line) and the experimental one (green squares) computed from the data in (a) as a function of the input frequency. (c) and (d) Time-domain traces measured by sensors T1 and T4 at points A (2 Hz, acoustic branch) and B (6 Hz, bandgap) as indicated in (a).

receive no advantage from traditional seismic isolation, whereas the CF filtering effect can indeed be effective. Therefore, metamaterial-based isolation is expected to have better isolation characteristics and be more widely applicable compared to standard SI.

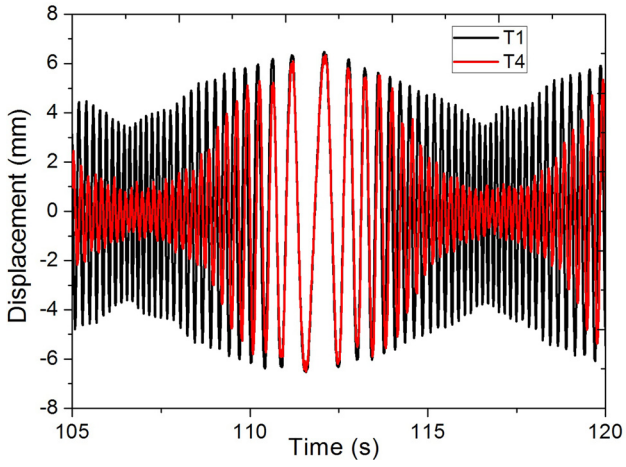

FIG. 6. Time-domain traces measured by sensors T1 (black line) and T4 (red line) for an input up/down chirp signal applied to layer 1. The signal frequency increases from 1 Hz to 8 Hz.

To compare the dynamical properties of a CF with and without resonators from a theoretical perspective, it is sufficient to consider a mass–spring periodic chain that is characterized by simpler expressions for the dispersion relationship and the attenuation coefficient, namely,

$$\begin{cases} m_e\omega^2 + 2k_e(1-\cos(qL)) = 0, \\ qL = a\cos\left(1 - \dfrac{m_e\omega^2}{2k_e}\right). \end{cases} \tag{10}$$

The mass–spring periodic chain exhibits only a Bragg region (dissipation mechanism due to the rubber) starting at a frequency around 8 Hz and in which the attenuation coefficient increases monotonically with no resonance. In other words, the internal resonance of the mass-in-mass periodic chain gives rise to a more-efficient attenuation mechanism that starts at a lower frequency than the mass–spring periodic chain (4.5 Hz as opposed to 8 Hz).

We also wish to stress that this seismic metamaterial does not exhibit a "negative refraction index." Rather, the effective mass depends on the frequency and becomes negative for frequencies within the bandgap.[14,17] In addition, the amount of physical space required for SI is comparable with

the size of the building itself, which is a key issue for any future commercialization (see Fig. 2).

V. SUMMARY AND CONCLUSIONS

New buildings should be developed to reduce shaking-related damage. To that end, we propose herein the concept of a CF with two properties, namely, the local resonance and a dual-stiffness structure,[23] i.e., large (small) rigidity for compression (shear) effects. This new design paradigm of CF retains the resistance of a standard foundation to a vertical load (i.e., a building on top), while offering the advantage of filtering the energy of S-waves propagating through it with frequencies within its bandgap. Specifically, our data show that S-waves with frequencies greater than 4.5 Hz (the starting frequency of the theoretical bandgap) are attenuated and that the device studied herein can filter more than 50% of the wave energy within that bandgap. We argue that this fundamental result on S-wave filtering could be the basis for designing a new generation of building-protection devices[24] that join seismic metamaterial concepts applied to surface and volume seismic waves. A challenge in developing this concept into a widespread alternative to standard foundations in new buildings will be to design a CF whereby the main resonance frequency of the building and the amplification region of the soil response are both within the bandgap.

SUPPLEMENTARY MATERIAL

See supplementary material for a video of the dynamic measurements of the CF.

ACKNOWLEDGMENTS

This work was supported by the SIES project (Strategic Initiatives for the Environment and Security), Progetto Premiale, funded by the Italian Ministry of Education, Universities and Research. The authors are thankful to Domenico Romolo for the support in preparing the figures and the staff of the Laboratory for Structural and Material Testing (MASTRLAB) of Politecnico di Torino for support in the experimental activities, in particular, Oronzo Pallara for setting up the data-acquisition system. The three-dimensional numerical simulations were performed using Abaqus licensed under a research agreement between Dassault Systèmes and G. Ventura at Politecnico di Torino. The simulations were performed with the computational facilities of PETASPIN (Petascale Spintronics computational laboratory) developed jointly by the University of Messina and INGV.

[1]V. G. Veselago, Sov. Phys. **10**, 509 (1968).
[2]J. B. Pendry, A. J. Holden, D. J. Robbins, and W. J. Stewart, IEEE Trans. Microwave Theory Tech. **47**, 2075 (1999).
[3]R. Craster and S. Guenneau, *Acoustic Metamaterials: Negative Refraction, Imaging, Lensing and Cloaking* (Springer, London, 2012).
[4]Z. Liu, X. Zhang, Y. Mao, Y. Y. Zhu, Z. Yang, C. T. Chan, and P. Sheng, Science **289**, 1734 (2000).
[5]S. Brûlé, E. H. Javelaud, S. Enoch, and S. Guenneau, Phys. Rev. Lett. **112**, 133901 (2014).
[6]A. Colombi, P. Roux, S. Guenneau, P. Gueguen, and R. V. Craster, Sci. Rep. **6**, 19238 (2016).
[7]M. Miniaci, A. Krushynska, F. Bosia, and N. M. Pugno, New J. Phys. **18**, 083041 (2016).
[8]Y. Yan, A. Laskar, Z. Cheng, F. Menq, Y. Tang, Y. L. Mo, and Z. Shi, J. Appl. Phys. **116**, 044908 (2014).
[9]N. Aravantinos-Zafiris and M. M. Sigalas, J. Appl. Phys. **118**, 064901 (2015).
[10]P. Cacciola and A. Tombari, Proc. R. Soc. A **471**, 20150075 (2015).
[11]C. C. Spyrakos, I. A. Koutromanos, and C. A. Maniatakis, Soil Dyn. Earthquake Eng. **29**, 658–668 (2009).
[12]S. Brûlé, E. H. Javelaud, S. Enoch, and S. Guenneau, Sci. Rep. **7**, 18066 (2017).
[13]S. Brûlé, S. Enoch, and S. Guenneau, preprint arXiv:1712.09115 (2017).
[14]H. H. Huang, C. T. Sun, and G. L. Huang, Int. J. Eng. Sci. **47**, 610–617 (2009).
[15]H. H. Huang and C. T. Sun, New J. Phys. **11**, 013003 (2009).
[16]S.-H. Kim and M. P. Das, Mod. Phys. Lett. B **26**, 1250105 (2012).
[17]G. Finocchio, O. Casablanca, G. Ricciardi, U. Alibrandi, F. Garescì, M. Chiappini, and B. Azzerboni, Appl. Phys. Lett. **104**, 191903 (2014).
[18]Y. Zhou, P. Wei, and Q. Tang, Acta Mech. **227**, 2361–2376 (2016).
[19]The 3-dimentional numerical simulations have been performed with Abaqus, licensed under research agreement between Dassault Systèmes and G. Ventura at Politecnico di Torino.
[20]F. Garesci, Int. J. Adhes. Adhes. **33**, 7–14 (2012).
[21]F. Garesci and S. Fliegener, Compos. Sci. Technol. **85**, 142–147 (2013).
[22]F. Levinzon, *Piezoelectric accelerometers with integral electronics* (Springer International Publishing, 2015).
[23]The concept of dual-stiffness structure introduced here is different from what proposed in previous works. See for example: Y.-J. Park, J. Gu Lee, S. Jeon, H. Ahn, J. Koh, J. Ryu, M. Cho, and K. Jin Cho, J. Intell. Mater. Syst. Struct. **27**, 995–1010 (2016).
[24]Y. Achaoui, B. Ungureanu, S. Enoch, S. Brûlé, and S. Guenneau, Extreme Mech. Lett. **8**, 30–37 (2016).